Physics and Imaging in Radiation Oncology 23 (2022) 8–15

Contents lists available at ScienceDirect

Physics and Imaging in Radiation Oncology

journal homepage: www.sciencedirect.com/journal/physics-and-imaging-in-radiation-oncology

Repeatability of radiotherapy dose-painting prescriptions derived from a multiparametric magnetic resonance imaging model of glioblastoma infiltration

Caterina Brighi [a,b,*], Niels Verburg [c,d], Eng-Siew Koh [b,e,f], Amy Walker [b,e,f], Cathy Chen [e], Sugendran Pillay [e,f,g], Philip C. de Witt Hamer [c,d], Farhannah Aly [b,e,f], Lois C. Holloway [b,e,f], Paul J. Keall [a,b], David E.J. Waddington [a,b]

[a] ACRF Image X Institute, Sydney School of Health Sciences, The University of Sydney, Sydney, Australia
[b] Ingham Institute for Applied Medical Research, Sydney, Australia
[c] Brain Tumor Center Amsterdam, Amsterdam UMC, Amsterdam, The Netherlands
[d] Department of Neurosurgery, Amsterdam UMC, Amsterdam, The Netherlands
[e] Liverpool and Macarthur Cancer Therapy Centres, Sydney, Australia
[f] South West Sydney Clinical Campus, University of New South Wales, Sydney, Australia
[g] Campbelltown Hospital, Sydney, Australia

ARTICLE INFO

Keywords:
Dose-painting
Multiparametric MRI
Repeatability
Glioblastoma
Radiotherapy

ABSTRACT

Background and purpose: Glioblastoma (GBM) patients have a dismal prognosis. Tumours typically recur within months of surgical resection and post-operative chemoradiation. Multiparametric magnetic resonance imaging (mpMRI) biomarkers promise to improve GBM outcomes by identifying likely regions of infiltrative tumour in tumour probability (TP) maps. These regions could be treated with escalated dose via dose-painting radiotherapy to achieve higher rates of tumour control. Crucial to the technical validation of dose-painting using imaging biomarkers is the repeatability of the derived dose prescriptions. Here, we quantify repeatability of dose-painting prescriptions derived from mpMRI.

Materials and methods: TP maps were calculated with a clinically validated model that linearly combined apparent diffusion coefficient (ADC) and relative cerebral blood volume (rBV) or ADC and relative cerebral blood flow (rBF) data. Maps were developed for 11 GBM patients who received two mpMRI scans separated by a short interval prior to chemoradiation treatment. A linear dose mapping function was applied to obtain dose-painting prescription (DP) maps for each session. Voxel-wise and group-wise repeatability metrics were calculated for parametric, TP and DP maps within radiotherapy margins.

Results: DP maps derived from mpMRI were repeatable between imaging sessions (ICC $>$ 0.85). ADC maps showed higher repeatability than rBV and rBF maps (Wilcoxon test, $p = 0.001$). TP maps obtained from the combination of ADC and rBF were the most stable (median ICC: 0.89).

Conclusions: Dose-painting prescriptions derived from a mpMRI model of tumour infiltration have a good level of repeatability and can be used to generate reliable dose-painting plans for GBM patients.

Abbreviations: ADC, apparent diffusion coefficient; DP, dose prescription; GBM, glioblastoma; ICC, intraclass correlation coefficient; CTV, clinical target volume; GTV, gross tumour volume; PTV, planned target volume; VOI, volume of interest; CSF, cerebrospinal fluid; mpMRI, multiparametric MRI; TP, tumour probability; rBV, relative cerebral blood volume; rBF, relative cerebral blood flow; DSC, dynamic-susceptibility contrast; T1CE, T_1-weighted post-contrast; FLAIR, fluid-attenuated inverse recovery; CV, coefficient of variation; RC, repeatability coefficient; σ_b^2, between-subject variance; σ_w^2, within-subject variance; ΔTP, difference in tumour probability between timepoint 2 and timepoint 1; SVZ, subventricular zones; EORTC, European Organisation for Research and Treatment of Cancer.

* Corresponding author at: Room 217, Level 2, Biomedical building (C81), 1 Central Avenue, Eveleigh, 2015 NSW, Australia.
E-mail address: caterina.brighi@sydney.edu.au (C. Brighi).

https://doi.org/10.1016/j.phro.2022.06.004
Received 20 March 2022; Received in revised form 6 June 2022; Accepted 8 June 2022
Available online 11 June 2022

1. Introduction

Glioblastoma (GBM) is the most aggressive type of brain cancer, with 5-year survival rate of 5.1% and the majority of recurrences occurring locally within months of first-line treatment [1,2]. A major limitation to the improvement of treatment for GBM is the lack of a means to predict regions with a high risk of local relapse. Local relapse is caused by the ability of the tumour to develop mechanisms of treatment resistance as occurs via the high level of biological heterogeneity in GBM. Such biological heterogeneity causes variations in tissue sensitivity to chemoradiation treatment, often via tissue hypoxia, and manifests as chaotic tumour growth and migration, variable cellular density and metabolism, and irregular and dysfunctional vascular architecture [3,4].

An emerging approach to address the high risk of local relapse due to biological heterogeneity is the prescription and delivery of a non-uniform radiation dose distribution based on physiological information of the tumour microenvironment – a concept known as dose-painting [5]. Dose-painting relies on the hypothesis that there is a predictable relationship between each tumour phenotype and the dose prescription that optimises local tumour control. For instance, GBM cells infiltration in the brain parenchyma is a treatment resistance mechanism responsible for tumour progression but is undetectable with anatomical MRI. Using functional information to identify patterns of likely tumour infiltration could enable optimisation of dose distribution and enable delivery of higher doses to likely region of relapse, thus increasing the likelihood of local control [4,5].

MRI is the core imaging modality in the management of GBM patients, for diagnosis, target delineation for surgery and radiation treatment, assessment of treatment response and disease progression [6,7]. However, radiotherapy planning solely relies on anatomical MRI data, which are limited in their ability to capture the biological heterogeneity of the tumour microenvironment [8].

Functional MRI techniques, including diffusion- and perfusion-weighted MRI, magnetic resonance spectroscopy (MRS) and blood-oxygen level dependent (BOLD) MRI, allow quantification of several aspects of the tumour physiology [9]. Combining two or more functional MRI techniques – a concept known as multiparametric MRI (mpMRI) – provides a means to spatially characterise biological heterogeneity within the brain and could be used to guide radiotherapy dose escalation in regions of infiltrating tumour [9–13].

Recently, a number of mpMRI models developed to predict the probability of tumour infiltration at each voxel in the tumour microenvironment have been reviewed by d'Este *et al* [14]. Only six of the 14 studies reviewed used histopathology from stereotactic biopsy as reference standard for tumour infiltration and, of these six, the study with the greatest accuracy combined multiparametric image intensities in a generalized linear mixed model [15].

Clinical translation of tumour probability models into radiotherapy planning will require validation that the probability maps truly reflect the presence of tumour infiltration (biological validation) and are repeatable and reproducible (technical validation) [16]. While studies focusing on the biological validation of new mpMRI models of tumour infiltration are prevalent in the current literature, technical validation studies are scarce [17]. However, MRI-derived parameters of diffusion/perfusion were previously shown to be predictive of the site of local relapse [15,18].

In this study, we aimed to evaluate repeatability of a biologically-validated mpMRI model of tumour infiltration combining MRI-derived parameters of diffusion and perfusion.

2. Materials and methods

2.1. Patient dataset

Imaging data were obtained from the QIN GBM Treatment Response collection publicly available on The Cancer Imaging Archive (TCIA) [19–22]. All data from TCIA are anonymised, thus individual institutional IRB approval was not required for this study. However, it should be noted that all data were originally submitted to TCIA by the contributing institutions under IRB-approved protocol. The dataset consisted of mpMRI images acquired for 11 newly diagnosed GBM patients in a test–retest study. Scans were acquired 2–6 days apart at 3–7 days and then 1 day prior to commencement of post-operative chemo-radiation treatment [23]. From the information available, we estimated that the imaging was performed 3–5 weeks post-surgery. Imaging sequences used in our study included structural T_1-weighted post-contrast (T1CE), fluid-attenuated inverse recovery (FLAIR), apparent diffusion coefficient (ADC) maps derived from diffusion-weighted MRI, and dynamic-susceptibility contrast (DSC) MRI sequences. An inclusion criterion for this study was availability of ADC maps and DSC MRI sequences at both imaging sessions, and only data from 11 of 54 patients from the QIN GBM Treatment Response collection fit this criterion (typically diffusion-weighted or DSC imaging was not available at one or both timepoints for excluded patients). Imaging data from each examination were analysed following a five-step workflow (Fig. 1). Image acquisition parameters and additional details of the workflow (**Fig. S1**) are in **Supplementary Material**.

2.2. Image pre-processing

Images were processed with nordicICE (v4.1.3, NordicNeuroLab, Norway) and FSL. The FLAIR, ADC and DSC images were rigidly registered to the T1CE image. Relative cerebral blood volume (rBV) and relative cerebral blood flow (rBF) maps were derived from perfusion modelling of DSC images following consensus recommendations for DSC MRI analysis in high-grade gliomas [22,24]. Images acquired at timepoint 2 were rigidly registered to images acquired at timepoint 1 [25,26]. Binary masks of the brain volume were generated and used to mask signal in the field of view of the DSC sequence acquisition. The ADC, rBV and rBF images were resampled to 1.2 mm isotropic resolution. DSC brain masks were applied to generate parametric maps only in regions of the brain where both diffusion- and perfusion-weighted data were acquired. ADC, rBF and rBF maps were normalised to a reference volume manually selected in the contralateral normal brain, smoothed with an edge-preserving bilateral filter, zeroed, centred and scaled, similarly to the method in Verburg *et al* [15]. Binary masks of the cerebrospinal fluid (CSF) volume were obtained from FLAIR images [27]. Additional details on image pre-processing steps are included in the **Supplementary Material**.

2.3. Volume of interest delineation

The gross tumour volume (GTV) was manually delineated by a radiation oncologist (F.A.) and reviewed by a second expert radiation oncologist (E-S.K.) on the T1CE image acquired at timepoint 1 in MIM (Cleveland, OH). Clinical target volume (CTV) expansions, representing the region at risk for microscopic tumour spread, were generated by applying a 2 cm expansion to the GTV [8]. The volume of interest (VOI) for the repeatability analysis was defined by algebraic subtraction of the GTV from the CTV. The VOI was masked sequentially with the DSC brain mask and the whole brain mask to ensure the VOI only included areas of the brain with a dose prescription value derived from the mpMRI TP.

2.4. Tumour probability modelling

After pre-processing, the ADC, rBV and rBF maps were linearly combined to generate TP maps as previously described [15]. Two types of TP maps were generated. ADC-rBV TP maps obtained from the combination of ADC and rBV maps. ADC-rBF TP maps obtained from the combination of ADC and rBF maps. The coefficients for optimal imaging combinations were determined with logistic regression analysis that combines the mean values of intensity in a region of interest surrounding

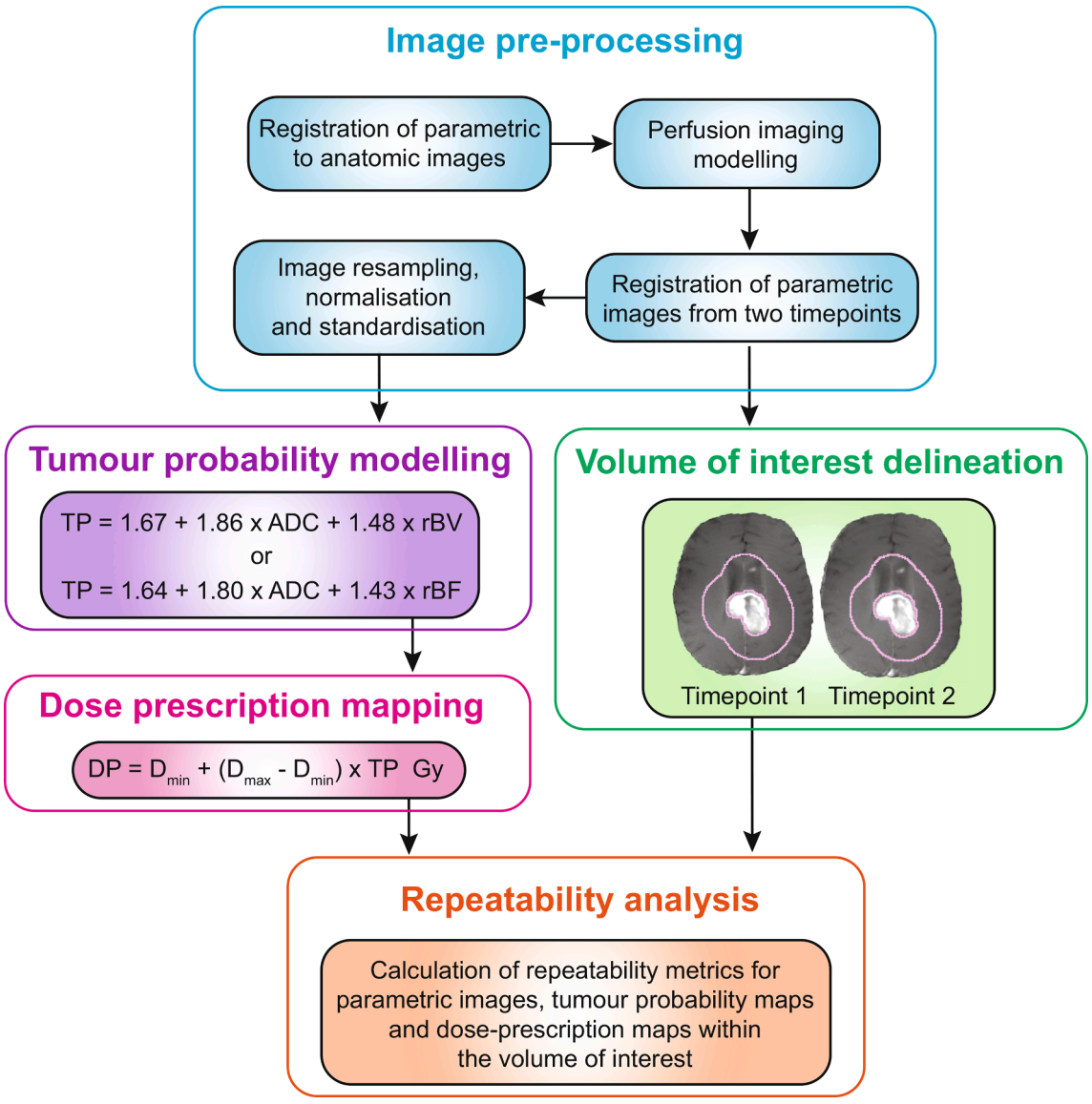

Fig. 1. *Schematic overview of the image analysis pipeline*. The pipeline involves five steps: *image pre-processing*, including registration of the parametric to the anatomical images, perfusion imaging modelling, registration of the parametric images from the two timepoints, image resampling, normalisation and standardisation; *tumour probability modelling*, according to the linear formula obtained from the regression analysis coefficients; *dose prescription mapping*, linearly mapping TP values to a dose prescription; *volume of interest delineation* from the gross tumour volume and the clinical target volume; *repeatability analysis*, with calculation of repeatability metrics for the parametric, TP and DP maps within the volume of interest. ADC, apparent diffusion coefficient; D_{max}, maximum dose; D_{min}, minimum dose; DP, dose prescription; rBF, relative blood flow; rBV, relative blood volume; TP, tumour probability.

the contrast-enhancing tumour mass to predict the probability of infiltrating tumour presence at each voxel. Methods and results (Table S1) of the logistic regression analysis are in **Supplementary Material**. Voxels within the GTV were, by definition, considered tumour and assigned a TP of 1. As the TP model was not designed to give accurate predictions in areas containing CSF (including cistern and sulci), these areas were removed from the final TP map by masking the TP map with the binary CSF mask and assigned a zero value. This step mitigated artifacts that resulted from intrinsically high values of ADC and perfusion parameters in regions containing CSF [15].

2.5. Dose prescription mapping

The TP for each voxel in the brain was translated into a dose prescription (DP) using a polynomial dose mapping function that physically determines the rate of conferred radio-resistance to cells in each voxel for a given TP [28]. Bowen *et al.* found that prescriptions based on low-order ($n < 2$) polynomial mapping functions result in a planned target dose that conforms to a greater percentage of the target volume [28]. Greater conformity is achievable because the plan optimisation process modulates only the steepness of dose gradients through the choice of a single parameter [28]. Hence, we chose a linear dose mapping function:

$$DP = D_{min} + (D_{max} - D_{min}) \times TP \ \ Gy$$

where D_{min} and D_{max} were the minimum and maximum prescribed dose, respectively. D_{min} was set to 60 Gy, reflecting the standard of care adjuvant radiation dose recommended by the EORTC guidelines for younger fit GBM patients [8]. D_{max} was set to 80 Gy, corresponding to the maximum tolerated dose considered safe as determined by the RTOG trial 98–03 [29]. RayStation treatment planning system (v.10B, RaySearch Laboratories) was used to develop dose-painting plans from DP at the two timepoints for three GBM patients with tumour near critical brain structures. The methods description for dose-painting plan creation is in **Supplementary Material**.

2.6. Repeatability analysis

Voxel-wise repeatability of the planning pipeline was assessed within the VOI for the parametric, TP and DP maps, and within the planning tumour volume (PTV) for the dose-painting plans, by means of intraclass correlation coefficient (ICC) and within-voxel coefficient of variation (CV). ICC was used to quantify the variability between voxels relative to the measurement error and was calculated with a two-way random effects, absolute agreement, single rater/measurement model [30,31] Poor, moderate, good and excellent repeatability was indicated by ICC values < 0.5, 0.5–0.75, 0.75–0.9, and > 0.90, respectively [32]. Within-voxel CV was calculated as per recommended statistical methods [33]. Patient-wise repeatability of mean values within the VOI was assessed for the parametric, TP and DP maps by means of Bland-Altman plots, between-subject variance (σ_b^2), within-subject variance (σ_w^2), ICC, within-subject CV and repeatability coefficient (RC), as per recommended statistical methods [33]. For patient-wise analysis, ICC represented the variability of two within-subject measurements relative to the variation between subjects. RC was determined from σ_w^2, and represented the estimated range of variation between the measurements so that the difference between two measurements was expected to be between -RC and RC for 95% of patients and reflected the amount of change that should occur to be considered significant and not be related to intra-method variability [34].

2.7. Statistical analysis

The difference in TP between timepoint 2 and timepoint 1 (ΔTP) was calculated for both ADC-rBF and ADC-rBV combinations. The comparison of the variances between ADC-rBF ΔTP and ADC-rBV ΔTP distributions was assessed via a F-test of the equality of two variances. The difference in voxel-wise ICC and within-voxel CV between a) ADC and rBV maps, b) ADC and rBF maps, and c) ADC-rBV DP and ADC-rBF DP maps was assessed via Wilcoxon matched-pairs signed rank test.

3. Results

ADC, rBV, rBV, TP and DP maps were similar between the two timepoints (Fig. 2). The TP histograms (Fig. 3) showed similar TP distributions between timepoints for both combinations ADC-rBV and ADC-rBF. The histograms of ΔTP also showed similar distributions with means 0.04 and 0.03 for ADC-rBV and ADC-rBF combinations, respectively. However, ADC-rBV TP ΔTP distribution had a larger variance than the ADC-rBF TP ΔTP distribution ($F = 1.17$, $p < 0001$). F-test results for all the patients are in Table S2 of **Supplementary Material**.

ICC values for ADC maps were on average 1.5 and 1.3 times higher ($p = 0.001$) than for rBV and rBF maps, respectively (Fig. 4**a**). Within-voxel CV values for ADC maps were on average 4 and 2.8 times lower ($p = 0.001$) than for rBV and rBF maps, respectively (Fig. 4**b**). TP maps had on average 1.3 times higher ($p = 0.001$) ICC values and 3 times lower ($p = 0.001$) within-voxel CV values than their respective perfusion

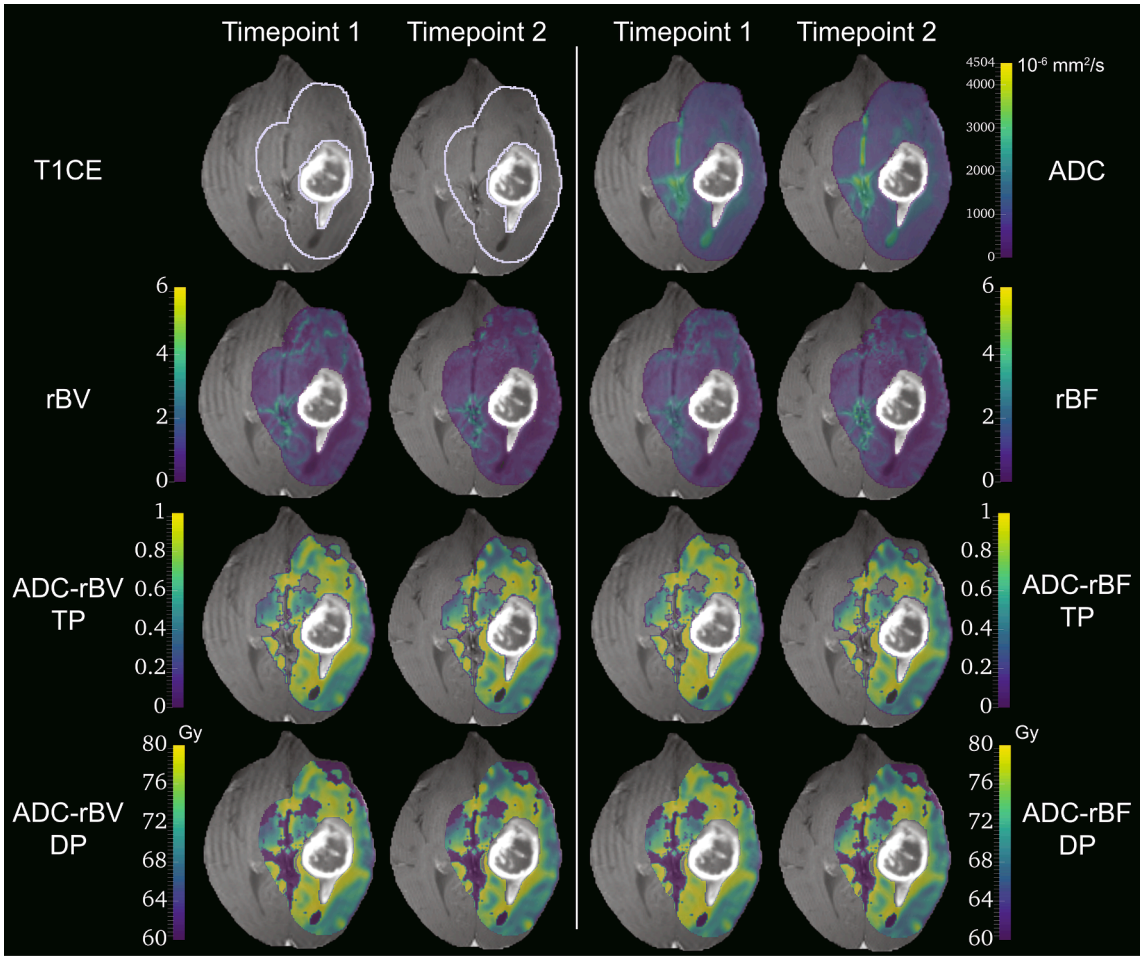

Fig. 2. *Comparison of MRI-derived parametric, tumour probability and dose prescription maps between two imaging sessions.* The figure displays left–right, top–bottom T1CE images from the two timepoints with overlayed a) volume of interest contours shown in purple, b) ADC maps, c) rBV maps, d) rBF maps, e) ADC-rBV TP maps, f) ADC-rBF TP maps, g) ADC-rBV DP maps, h) ADC-rBF DP maps. T1CE, T1-weighted contrast enhanced image; ADC, apparent diffusion coefficient; DP, dose prescription; rBF, relative blood flow; rBV, relative blood volume; TP, tumour probability.

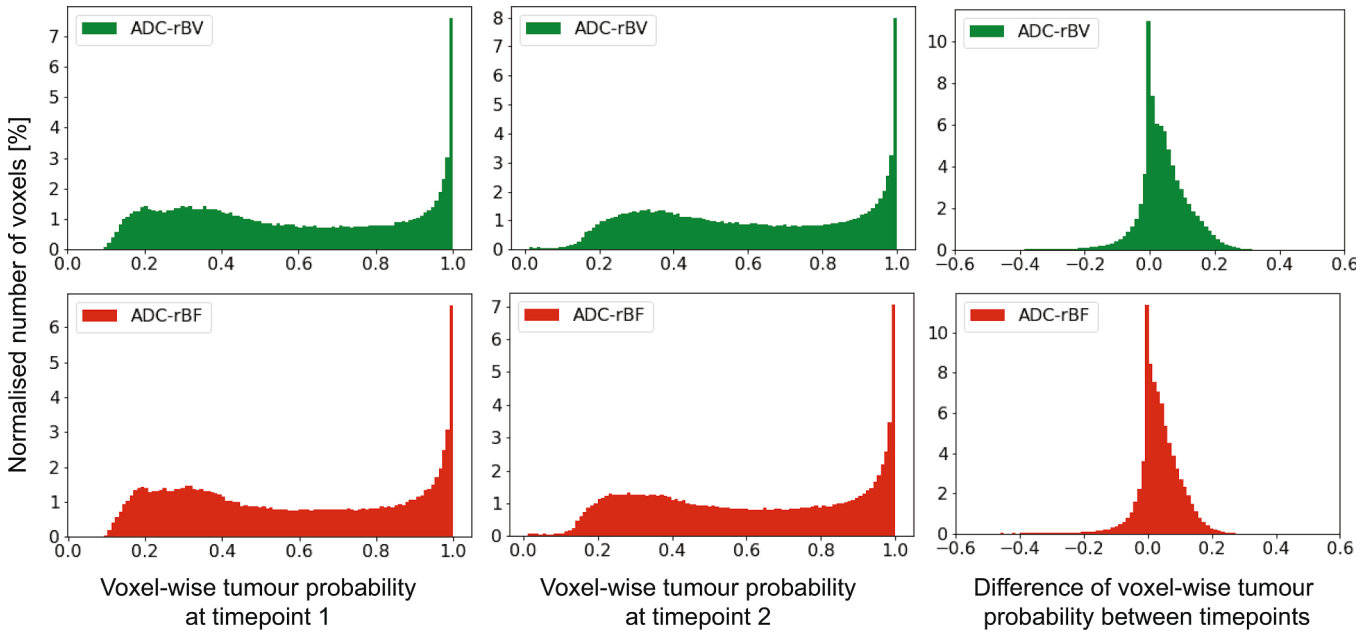

Fig. 3. *Example of histograms of voxel-wise tumour probability.* The figure displays top–bottom, normalised histograms of the distributions of ADC-rBV (top) and ADC-rBF (bottom) voxel-wise tumour probability at timepoint 1 (left), at timepoint 2 (centre) and difference of voxel-wise tumour probability between timepoint 2 and timepoint 1. ADC, apparent diffusion coefficient; rBF, relative blood flow; rBV, relative blood volume. Bin size: 100.

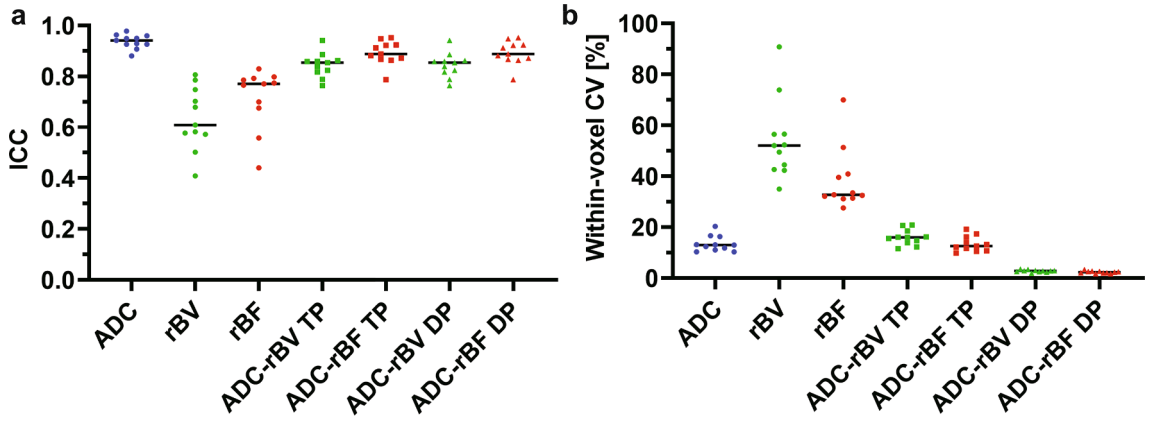

Fig. 4. *Voxel-wise repeatability metrics.* The figure displays in **a|** ICC values and in **b|** within-voxel CV values of the parametric, TP and DP maps obtained from the voxel-wise repeatability analysis. ADC, apparent diffusion coefficient; CV, coefficient of variation; DP, dose prescription, ICC, intraclass correlation coefficient; rBF, relative blood flow; rBV, relative blood volume; TP, tumour probability. Bars represent the median values from the 11 GBM patients.

parametric maps (Fig. 4). DP maps had on average 5.8 times lower ($p = 0.001$) within-voxel CV values than their respective TP maps (Fig. 4**b**). ADC-rBF DP maps had 1.1 times higher ($p = 0.001$) values of ICC and 1.2 times lower ($p = 0.001$) values of within-voxel CV than ADC-rBV DP maps ($p = 0.001$).

Bland–Altman plots of the parametric, TP and DP maps (Fig. 5) showed good agreement between the two measurements with all values within the limits of agreement for each parameter, except for one value in rBV and rBF maps. A positive bias of $6{\cdot}10^{-6}$ mm^2/s, 0.3 and 0.1 was observed for ADC, rBV and rBF maps, respectively. A negative bias of −0.01 and −0.2 was observed for TP and DP maps, respectively. Table 1 reports metrics of repeatability evaluated at the patient level. These results showed similar trends to those observed for the voxel-wise analysis, with ICC and within-subject CV values improving throughout the image analysis and modelling pipeline.

ICC values within the PTV were on average higher by 0.05 for the dose-painting plans than for their respective ADC-rBF DP (**Fig. S2**).

4. Discussion

Our results demonstrate that dose-painting prescriptions derived from a mpMRI model of tumour infiltration have a good level of repeatability and can be used to generate reliable dose-painting plans.

To our knowledge, this is the first study that reports repeatability metrics of mpMRI-derived TP and DP maps in GBM. We assessed metrics of repeatability in ADC, rBV and rBF parameters, and in TP and DP maps in the entire region relevant for radiotherapy planning, finding results consistent with previous studies where repeatability metrics were evaluated solely for ADC, rBV and rBF parameters in regions of T_1-weighted contrast enhancement and regions of FLAIR-hyperintensity [21,22,35]. We limited the TP repeatability analysis solely to the volume of tissue which extends from the GTV to the CTV as this is the region in which the mpMRI model was validated [15]. Additionally, this peritumoural region has the highest likelihood of tumour infiltration and, thus, is most relevant to the prescription of a heterogeneous radiation dose distribution. We applied the model to post-operative images

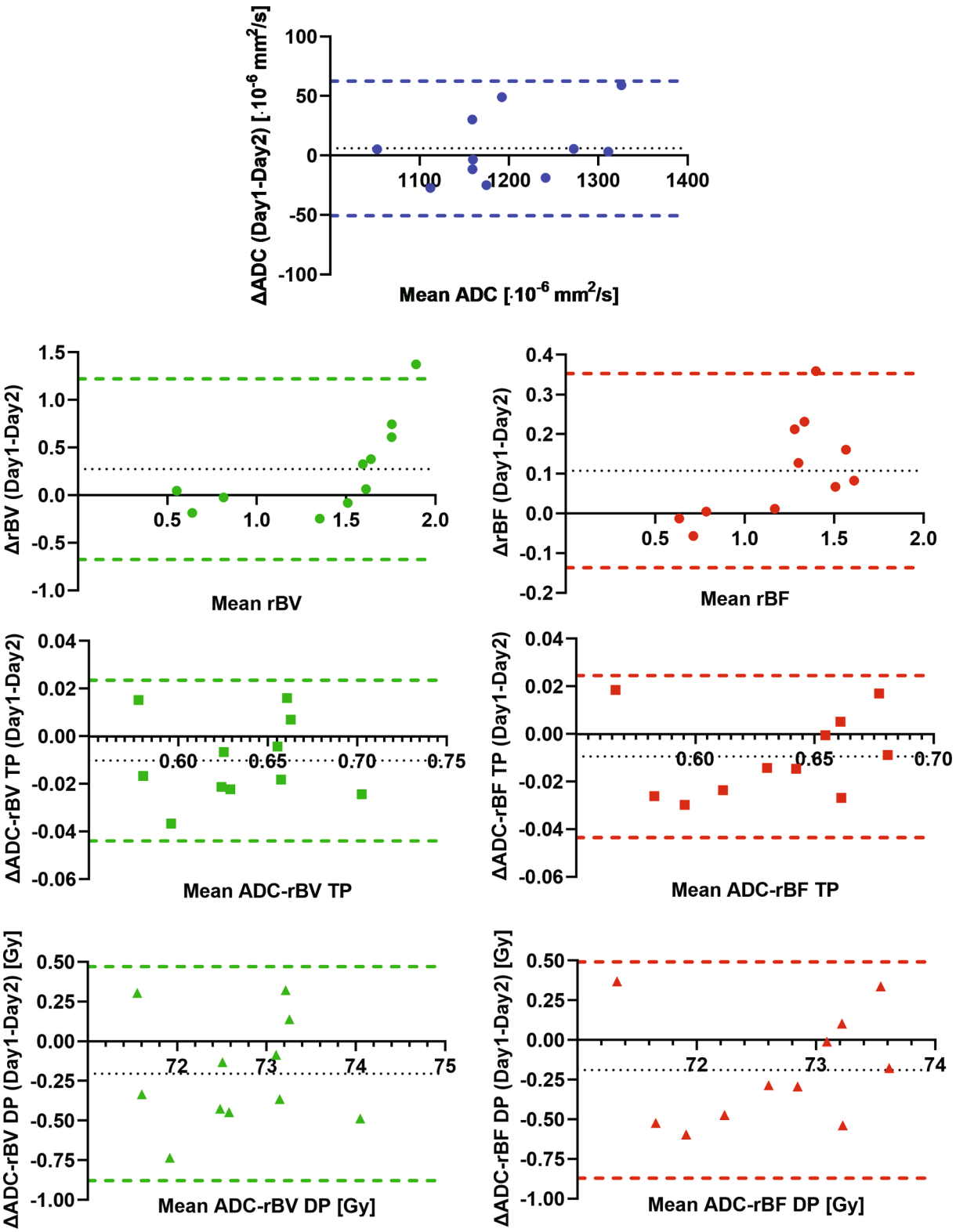

Fig. 5. *Bland–Altman plots for analysis of repeatability*. The figure displays the Bland-Altman plots of the mean ADC values (top); mean rBV, mean ADC-rBV TP and mean ADC-rBV DP (left); mean rBF, mean ADC-rBF TP and mean ADC-rBF DP (right) calculated from the volume of interest-based repeatability analysis. ADC, apparent diffusion coefficient; DP, dose prescription; rBF, relative blood flow; rBV, relative blood volume; TP, tumour probability. Coloured dotted lines represent limits of agreement. Black dotted lines represent bias.

acquired at a timepoint where radiological changes have typically stabilised [36]. We note that the TP model is not applicable in the GTV, which is, by definition, tumour with a TP of 1.

Potentially, dose-painting plans for GBM patients could prescribe a dose boost within the remaining tumour (GTV) and the surrounding area where > 90% GBM recurrences occur with a DP guided by the underlying probability of tumour infiltration within the CTV. With this approach, we found that dose-painting plans can be feasibly generated

Table 1
Patient-wise metrics of repeatability.*

Image type	σ_b^2	σ_w^2	ICC	within-subject CV %	RC(RC_U-RC_L)
ADC	6179 (10^{-6} $mm^2/s)^2$	397 (10^{-6} $mm^2/s)^2$	0.94	1.7	55 (94–39) 10^{-6} mm^2/s
rBV	0.14	0.14	0.48	27.6	1.05 (1.78–0.74)
rBF	0.10	0.01	0.89	9.4	0.31 (0.53–0.22)
ADC-rBV TP	0.00	0.00	0.87	2.2	0.04 (0.06–0.03)
ADC-rBF TP	0.00	0.00	0.88	2.1	0.04 (0.06–0.03)
ADC-rBV DP	0.51 Gy^2	0.07 Gy^2	0.87	0.4	0.76 (1.29–0.54) Gy
ADC-rBF DP	0.51 Gy^2	0.07 Gy^2	0.88	0.4	0.75 (1.27–0.53) Gy

[1] σ_b^2, between-subject variance; σ_w^2, within-subject variance; ICC, intraclass correlation coefficient; RC, repeatability coefficient; RC_L, lower RC confidence interval; RC_U, upper RC confidence interval; CV, coefficient of variation.

with high repeatability, even in cases of GBM patients where the tumour is in a challenging location adjacent to critical brain structures. Additionally, we observed that ICC values within the PTV were higher for the dose-painting plans than for their respective DP, likely due to increased blurring of dose in treatment plans when compared to DP [37].

Clinical evidence shows that GBM patients with tumours adjacent to the subventricular zones (SVZ) have inferior outcomes in terms of median overall survival, time to progression, and recurrence, and that increasing radiation dose to SVZ adjacent to the tumour correlates with better survival outcomes [38–41]. Interestingly, TP maps for the example shown in Fig. 2 showed that the highest probability of tumour infiltration was in proximity to the GTV edge, which reflects known GBM patterns of neural stem cell infiltration, in SVZ adjacent to the tumour, and in the cortex [42–45]. The higher radiation dose prescribed to these regions with the formulation used in this study might help improve local control. High values of TP in the cortex are likely due to artifacts created by intrinsically higher values of rBV/rBF in this region and could be addressed through modifications to the mpMRI TP model.

Our work shows that metrics of repeatability in TP and DP derived from a mpMRI model of tumour infiltration differ from repeatability metrics of the underlying ADC, rBV and rBF maps. Given that DP will impact patient treatment directly, testing DP repeatability is crucial to the clinical translation of mpMRI-derived models even when underlying parametric maps are repeatable. The higher repeatability of ADC maps than rBV/rBF maps likely reflects the fact that tumour tissue microstructural changes associated with cell death occur at a slower timescale than tumour tissue microvasculature changes, and ADC values are less susceptible than rBV/rBF to factors influencing the vascular bed. Further, rBV/rBF maps involve perfusion modelling with several operator-influenced variables that result in signal variations. The lower repeatability in ADC-rBV DP maps than in ADC-rBF DP maps is likely due to microvasculature changes occurring between the two scan sessions [46]. The systematic positive bias in the parametric maps reflects a slight decrease in values of ADC, rBV and rBF from the first imaging session, indicating the presence of biological changes in the VOI between the two imaging sessions.

The lack of validation of this mpMRI model of tumour infiltration in regions of CSF, cortex and SVZ, which reflects the practical challenges of obtaining image-guided biopsies from these brain regions, is a limitation of this study that must be overcome before this model is used in dose-painting clinical trials. Nonetheless, this study represents an important steppingstone towards the improvement and translation of this and any other mpMRI model for dose-painting, demonstrating that reliable DP can be obtained from the combination of functional MRI parameters. An additional important future step for technical validation of this and any other mpMRI model for dose-painting is evaluating reproducibility of DP maps generated from mpMRI images acquired for the same group of patients on multiple diagnostic systems.

Future development of this work will use ADC-rBF DP maps to generate dose-painting plans, building a workflow to implement the use of the DP map as an objective function for plan optimisation in a commercial treatment planning system and evaluating, with a post-hoc planning study, whether dose-painting would lead to improvements in modelled tumour control probability compared to conventional radiotherapy. While we used a simple linear mapping function to convert TP into DP values, it is likely that tumour control probability models combining image-derived biological information with tumour-specific radiobiological parameters of treatment response will lead to improved formulations to derive optimal DP in the future.

In conclusion, our workflow fills an important gap in the clinical translational pathway of image-guided dose-painting radiotherapy in GBM, providing a technical validation framework that can be used to evaluate the practical application of any emerging mpMRI model.

Funding

National Health and Medical Research Council (Grant numbers: APP1132471 and APP1194004).
Dutch Cancer Society (Grant number: #OAA/H1/VU 2015–7502).
Cancer Center Amsterdam (Grant number #2012–2-05).
Cancer Institute NSW ECF/1015.

Declaration of Competing Interest

The authors declare that they have no known competing financial interests or personal relationships that could have appeared to influence the work reported in this paper.

Appendix A. Supplementary data

Supplementary data to this article can be found online at https://doi.org/10.1016/j.phro.2022.06.004.

References

[1] Ostrom QT, Gittleman H, Fulop J, Liu M, Blanda R, Kromer C, et al. CBTRUS Statistical Report: Primary Brain and Central Nervous System Tumors Diagnosed in the United States in 2008-2012. Neuro Oncol 2015;17:iv1–62. https://doi.org/10.1093/neuonc/nov189.
[2] Stupp R, Mason WP, van den Bent MJ, Weller M, Fisher B, Taphoorn MJB, et al. Radiotherapy plus Concomitant and Adjuvant Temozolomide for Glioblastoma. N Engl J Med 2005;352:987–96. https://doi.org/10.1056/NEJMoa043330.
[3] Bonavia R, Inda MDM, Cavenee WK, Furnari FB. Heterogeneity maintenance in glioblastoma: A social network. Cancer Res 2011;71:4055–60. https://doi.org/10.1158/0008-5472.CAN-11-0153.
[4] Thorwarth D. Biologically adapted radiation therapy. Z Med Phys 2018;28:177–83. https://doi.org/10.1016/j.zemedi.2017.08.001.
[5] Ling CC, Humm J, Larson S, Amols H, Fuks Z, Leibel S, et al. Towards multidimensional radiotherapy (MD-CRT): Biological imaging and biological conformality. Int J Radiat Oncol Biol Phys 2000;47:551–60. https://doi.org/10.1016/S0360-3016(00)00467-3.
[6] Wen PY, Weller M, Lee EQ, Alexander BM, Barnholtz-Sloan JS, Barthel FP, et al. Glioblastoma in adults: A Society for Neuro-Oncology (SNO) and European Society of Neuro-Oncology (EANO) consensus review on current management and future directions. Neuro Oncol 2020;22:1073–113. https://doi.org/10.1093/neuonc/noaa106.
[7] Pope WB, Brandal G. Conventional and advanced magnetic resonance imaging in patients with high-grade glioma. Q J Nucl Med Mol Imaging 2018;62:239–53. https://doi.org/10.23736/S1824-4785.18.03086-8.
[8] Niyazi M, Brada M, Chalmers AJ, Combs SE, Erridge SC, Fiorentino A, et al. ESTRO-ACROP guideline "target delineation of glioblastomas". Radiother Oncol 2016;118:35–42. https://doi.org/10.1016/j.radonc.2015.12.003.
[9] Castellano A, Bailo M, Cicone F, Carideo L, Quartuccio N, Mortini P, et al. Advanced Imaging Techniques for Radiotherapy Planning of Gliomas. Cancers (Basel) 2021;13:1063. https://doi.org/10.3390/cancers13051063.
[10] Lupo JM, Nelson SJ. Advanced Magnetic Resonance Imaging Methods for Planning and Monitoring Radiation Therapy in Patients With High-Grade Glioma. Semin

Radiat Oncol 2014;24:248–58. https://doi.org/10.1016/j.semradonc.2014.06.008.
[11] Hu LS, Hawkins-Daarud A, Wang L, Li J, Swanson KR. Imaging of intratumoral heterogeneity in high-grade glioma. Cancer Lett 2020;477:97–106. https://doi.org/10.1016/j.canlet.2020.02.025.
[12] O'Connor JPB, Rose CJ, Waterton JC, Carano RAD, Parker GJM, Jackson A. Imaging intratumor heterogeneity: Role in therapy response, resistance, and clinical outcome. Clin Cancer Res 2015;21:249–57. https://doi.org/10.1158/1078-0432.CCR-14-0990.
[13] Keall PJ, Brighi C, Glide-Hurst C, Liney G, Liu PZY, Lydiard S, et al. Integrated MRI-guided radiotherapy — opportunities and challenges. Nat Rev Clin Oncol 2022. https://doi.org/10.1038/s41571-022-00631-3.
[14] d'Este SH, Nielsen MB, Hansen AE. Visualizing Glioma Infiltration by the Combination of Multimodality Imaging and Artificial Intelligence, a Systematic Review of the Literature. Diagnostics 2021;11:592. https://doi.org/10.3390/diagnostics11040592.
[15] Verburg N, Koopman T, Yaqub MM, Hoekstra OS, Lammertsma AA, Barkhof F, et al. Improved detection of diffuse glioma infiltration with imaging combinations: a diagnostic accuracy study. Neuro Oncol 2020;22:412–22. https://doi.org/10.1093/neuonc/noz180.
[16] O'Connor JPB, Aboagye EO, Adams JE, Aerts HJWL, Barrington SF, Beer AJ, et al. Imaging biomarker roadmap for cancer studies. Nat Rev Clin Oncol 2017;14:169–86. https://doi.org/10.1038/nrclinonc.2016.162.
[17] van Houdt PJ, Saeed H, Thorwarth D, Fuller CD, Hall WA, McDonald BA, et al. Integration of quantitative imaging biomarkers in clinical trials for MR-guided radiotherapy: Conceptual guidance for multicentre studies from the MR-Linac Consortium Imaging Biomarker Working Group. Eur J Cancer 2021;153:64–71. https://doi.org/10.1016/j.ejca.2021.04.041.
[18] C. Le Fèvre J.-M. Constans I. Chambrelant D. Antoni C. Bund B. Leroy-Freschini et al. Pseudoprogression versus true progression in glioblastoma patients: A multiapproach literature review. Part 2 – Radiological features and metric markers Crit Rev Oncol Hematol 2021;159:103230. 10.1016/j.critrevonc.2021.103230.
[19] Mamonov A-B-K-C-J. Data From QIN GBM Treatment Response. Cancer Imaging Arch 2016. https://doi.org/10.7937/k9/tcia.2016.nQF4gpn2.
[20] Clark K, Vendt B, Smith K, Freymann J, Kirby J, Koppel P, et al. The cancer imaging archive (TCIA): Maintaining and operating a public information repository. J Digit Imaging 2013;26:1045–57. https://doi.org/10.1007/s10278-013-9622-7.
[21] Prah MA, Stufflebeam SM, Paulson ES, Kalpathy-Cramer J, Gerstner ER, Batchelor TT, et al. Repeatability of Standardized and Normalized Relative CBV in Patients with Newly Diagnosed Glioblastoma. Am J Neuroradiol 2015;36:1654–61. https://doi.org/10.3174/ajnr.A4374.
[22] Jafari-Khouzani K, Emblem KE, Kalpathy-Cramer J, Bjørnerud A, Vangel MG, Gerstner ER, et al. Repeatability of Cerebral Perfusion Using Dynamic Susceptibility Contrast MRI in Glioblastoma Patients. Transl Oncol 2015;8:137–46. https://doi.org/10.1016/j.tranon.2015.03.002.
[23] Batchelor TT, Gerstner ER, Emblem KE, Duda DG, Kalpathy-cramer J. Improved tumor oxygenation and survival in glioblastoma patients who show increased blood perfusion after cediranib and chemoradiation. PNAS 2013;110:19059–64. https://doi.org/10.1073/pnas.1318022110.
[24] Boxerman JL, Quarles CC, Hu LS, Erickson BJ, Gerstner ER, Smits M, et al. Consensus recommendations for a dynamic susceptibility contrast MRI protocol for use in high-grade gliomas. Neuro Oncol 2020;22:1262–75. https://doi.org/10.1093/neuonc/noaa141.
[25] Jenkinson M, Smith S. A global optimisation method for robust affine registration of brain images. Med Image Anal 2001;5:143–56. https://doi.org/10.1016/S1361-8415(01)00036-6.
[26] Jenkinson M, Bannister P, Brady M, Smith S. Improved optimization for the robust and accurate linear registration and motion correction of brain images. Neuroimage 2002;17:825–41. https://doi.org/10.1016/S1053-8119(02)91132-8.
[27] Zhang Y, Brady M, Smith S. Segmentation of brain MR images through a hidden Markov random field model and the expectation-maximization algorithm. IEEE Trans Med Imaging 2001;20:45–57. https://doi.org/10.1109/42.906424.
[28] Bowen SR, Flynn RT, Bentzen SM, Jeraj R. On the sensitivity of IMRT dose optimization to the mathematical form of a biological imaging-based prescription function. Phys Med Biol 2009;54:1483–501. https://doi.org/10.1088/0031-9155/54/6/007.
[29] Tsien C, Moughan J, Michalski JM, Gilbert MR, Purdy J, Simpson J, et al. Phase I Three-Dimensional Conformal Radiation Dose Escalation Study in Newly Diagnosed Glioblastoma: Radiation Therapy Oncology Group Trial 98–03. Int J Radiat Oncol Biol Phys 2009;73:699–708. https://doi.org/10.1016/j.ijrobp.2008.05.034.
[30] de Vet HCW, Terwee CB, Knol DL, Bouter LM. When to use agreement versus reliability measures. J Clin Epidemiol 2006;59:1033–9. https://doi.org/10.1016/j.jclinepi.2005.10.015.
[31] Shrout PE, Fleiss JL. Intraclass correlations: Uses in assessing rater reliability. Psychol Bull 1979;86:420–8. https://doi.org/10.1037/0033-2909.86.2.420.
[32] Koo TK, Li MY. A Guideline of Selecting and Reporting Intraclass Correlation Coefficients for Reliability Research. J Chiropr Med 2016;15:155–63. https://doi.org/10.1016/j.jcm.2016.02.012.
[33] Raunig DL, McShane LM, Pennello G, Gatsonis C, Carson PL, Voyvodic JT, et al. Quantitative imaging biomarkers: A review of statistical methods for technical performance assessment. Stat Methods Med Res 2015;24:27–67. https://doi.org/10.1177/0962280214537344.
[34] Barnhart HX, Barboriak DP. Applications of the repeatability of quantitative imaging biomarkers: A review of statistical analysis of repeat data sets. Transl Oncol 2009;2:231–5. https://doi.org/10.1593/tlo.09268.
[35] Paldino MJ, Barboriak D, Desjardins A, Friedman HS, Vredenburgh JJ. Repeatability of quantitative parameters derived from diffusion tensor imaging in patients with glioblastoma multiforme. J Magn Reson Imaging 2009;29:1199–205. https://doi.org/10.1002/jmri.21732.
[36] Champ CE, Siglin J, Mishra MV, Shen X, Werner-Wasik M, Andrews DW, et al. Evaluating changes in radiation treatment volumes from post-operative to same-day planning MRI in High-grade gliomas. Radiat Oncol 2012;7:1–8. https://doi.org/10.1186/1748-717X-7-220.
[37] van Schie MA, Steenbergen P, Dinh CV, Ghobadi G, van Houdt PJ, Pos FJ, et al. Repeatability of dose painting by numbers treatment planning in prostate cancer radiotherapy based on multiparametric magnetic resonance imaging. Phys Med Biol 2017;62:5575–88. https://doi.org/10.1088/1361-6560/aa75b8.
[38] Lim DA, Cha S, Mayo MC, Chen MH, Keles E, Vandenberg S, et al. Relationship of glioblastoma multiforme to neural stem cell regions predicts invasive and multifocal tumor phenotype. Neuro Oncol 2007;9:424–9. https://doi.org/10.1215/15228517-2007-023.
[39] Chaichana KL, McGirt MJ, Frazier J, Attenello F, Guerrero-Cazares H, Quinones-Hinojosa A. Relationship of glioblastoma multiforme to the lateral ventricles predicts survival following tumor resection. J Neurooncol 2008;89:219–24. https://doi.org/10.1007/s11060-008-9609-2.
[40] Chen L, Chaichana KL, Kleinberg L, Ye X, Quinones-Hinojosa A, Redmond K. Glioblastoma recurrence patterns near neural stem cell regions. Radiother Oncol 2015;116:294–300. https://doi.org/10.1016/j.radonc.2015.07.032.
[41] Chen L, Guerrero-Cazares H, Ye X, Ford E, McNutt T, Kleinberg L, et al. Increased Subventricular Zone Radiation Dose Correlates With Survival in Glioblastoma Patients After Gross Total Resection. Int J Radiat Oncol 2013;86:616–22. https://doi.org/10.1016/j.ijrobp.2013.02.014.
[42] Smith AW, Mehta MP, Wernicke AG. Neural stem cells, the subventricular zone and radiotherapy: implications for treating glioblastoma. J Neurooncol 2016;128:207–16. https://doi.org/10.1007/s11060-016-2123-z.
[43] Sanai N, Alvarez-Buylla A, Berger MS. Neural Stem Cells and the Origin of Gliomas. N Engl J Med 2005;353:811–22. https://doi.org/10.1056/NEJMra043666.
[44] Barani IJ, Benedict SH, Lin P-S. Neural Stem Cells: Implications for the Conventional Radiotherapy of Central Nervous System Malignancies. Int J Radiat Oncol 2007;68:324–33. https://doi.org/10.1016/j.ijrobp.2007.01.033.
[45] Kut C, Janson RK. New Considerations in Radiation Treatment Planning for Brain Tumors: Neural Progenitor Cell-Containing Niches. Semin Radiat Oncol 2014;24:265–72. https://doi.org/10.1016/j.semradonc.2014.06.007.
[46] Hua J, Liu P, Kim T, Donahue M, Rane S, Chen JJ, et al. MRI techniques to measure arterial and venous cerebral blood volume. Neuroimage 2019;187:17–31. https://doi.org/10.1016/j.neuroimage.2018.02.027.